香港天文台
HONG KONG OBSERVATORY

Reprint 1025

Application of optical-flow technique to significant convection nowcast for terminal areas in Hong Kong

P. Cheung & H.Y. Yeung

The 3rd WMO International Symposium on Nowcasting and Very Short-Range Forecasting (WSN12), Rio de Janeiro, Brazil
6-10 August 2012

APPLICATION OF OPTICAL-FLOW TECHNIQUE TO SIGNIFICANT CONVECTION NOWCAST FOR TERMINAL AREAS IN HONG KONG

*P. Cheung and H.Y. Yeung**
Hong Kong Observatory, Hong Kong, China

ABSTRACT

The Hong Kong Observatory nowcasting system SWIRLS (Short-range Warning of Intense Rainstorms in Localized Systems) has been in operation since 1999. This is a robust and well-tested system that had been deployed in various places including Beijing, China for the Beijing 2008 Forecast Demonstration Project (B08FDP), Shanghai, China for the 2010 Shanghai World EXPO, New Delhi, India for the 19th Commonwealth Games, and Shenzhen, China for the 2011 Universiade. SWIRLS had undergone a major upgrade to version 2.0 in 2010 to use an optical-flow based tracking algorithm. Lately in 2011, the SWIRLS products had also been utilized to provide convection nowcast at the Hong Kong International Airport for the aviation community.

In this paper, the optical-flow techniques and various other tracking methods used and being tested in SWIRLS are discussed. The latest use of SWIRLS products in convection nowcast for aviation is described and the verification results presented. Limitations in the current implementation and future development effort are also discussed.

1. INTRODUCTION

In the literature of computer vision, the term "optical flow" usually refers to the velocity pattern of the apparent motion of moving objects in a visual scene when projected onto a two-dimensional plane, e.g. the film of a video camera (Aubert *et al*. 1999). Optical flow as an image processing technique finds its applications in many areas of computer vision, e.g. motion detection, object segmentation, time-to-collision and focus of expansion calculations, motion compensated encoding, stereo disparity measurement, etc. (Beauchemin & Barron 1995).

There are many different approaches and methods in the literature to solve for the optical flow. They can be divided into three main categories, namely local differential, global variational and phase-based. These three approaches to optical flow are introduced by Lucas and Kanade (1981), Horn and Schunck (1981) and Fleet and Jepson (1990) respectively. While both the local and global approaches rely on the brightness constancy assumption (to be explained in the next section), the phase-based approach resorts to a phase constancy assumption. The present paper will limit the scope of discussion to the first two approaches only. For the rest of this paper, "optical flow" refers approaches based on the brightness constancy assumption.

In the meteorological community, Laroche and Zawadzki (1994; 1995) independently developed a technique called Variational Echo Tracking (VET) to retrieve 3-dimensional wind field from clear-air radar echoes. The technique was later generalized by Germann and Zawadzki (2002) to track the motion of precipitation echoes over continental-scale radar composite images. The basic assumption of Lagrangian persistency in VET is essentially the same as the brightness constancy assumption in optical flow.

Bowler *et al*. (2004; 2006) also applied the optical flow constraint when developing an improved radar-echo tracking method for the Gandolf and later the STEPS nowcasting system. Instead of a variational approach with a single global minimization, the velocity field is obtained through several steps. Firstly, the radar rain rate field is divided into blocks and the velocity that best satisfies the optical flow equation is estimated for each block using a least squares approach. A smoothness constraint is then applied to the block velocities as a weighted averaging over the eight nearest neighbours of a block.

At the Hong Kong Observatory, Wong *et al*. (2009) introduced a Multi-scale Optical-flow by Variational Analysis (MOVA) scheme to improve the tracking of radar echoes when developing the second-generation SWIRLS nowcasting system (Yeung *et al*. 2009). MOVA had been applied in SWIRLS to

* *Corresponding author address*: Linus H.Y. Yeung, Hong Kong Observatory, 134A, Nathan Road, Kowloon, Hong Kong, China; e-mail: hyyeung@hko.gov.hk

support various international events, including the 2008 Beijing Olympic (Yeung *et al.* 2009; Wong *et al.*. 2009), the 2010 Shanghai World EXPO (WMO 2012), as well as the 2010 Commonwealth Games in New Delhi, India (Srivastava *et al.* 2012). Starting from 2010, MOVA has become the operation radar tracking scheme for quantitative precipitation forecast (QPF) of SWIRLS in Hong Kong. In recent years, the SWIRLS system has been adopted to provide thunderstorm and lightning alerting service for the Hong Kong International Airport (Li & Lau 2008). Lately in 2011, selected nowcast products from SWIRLS have been applied to the forecasting of significant convection for the aviation community.

In this paper, the mathematical formulations of optical flow technique relevant to the present study will be described in Section 2. Section 3 will present the implementation details of the various tracking algorithms available in SWIRLS. The significant convection nowcast products for aviation application in Hong Kong and the corresponding nowcasting support will be introduced in Section 4. Their performance during the summer months in 2011 will be presented in Section 4.2. The shortcomings in the present implementation and the design of further study will be discussed in Section 5. Section 6 concludes the present results and outline possible future works.

2. OPTICAL FLOW TECHNIQUE

The apparent motion of moving objects in a visual scene may be traced by examining the temporal changes in brightness or intensity $I(x,y,t)$ projected on a 2-dimensional plane, where (x,y) refers to the Cartesian coordinates on the plane and t is time. The corresponding optical flow can be deduced if one assumes that the intensity of a point on an object remains constant along its trajectory, i.e. the total derivative of $I(x,y,t)$ being zero. Mathematically, this translates to the following optical flow constraint (OFC) equation:

$$\frac{\partial I}{\partial t}+u\frac{\partial I}{\partial x}+v\frac{\partial I}{\partial y}=0 \tag{1}$$

The vector field (u,v) that satisfies Eq.(1) is called optical flow. Since there are two unknowns but just one constraining equation, there is no unique solution to Eq.(1). This issue is termed the aperture problem. To circumvent this problem, various additional constraints were proposed resulting in different algorithms and solutions to the OFC equation (see Aubert *et al.* (1999) for a review). Described below are several algorithms relevant to the present study.

The classical approach was pioneered by Horn and Schunck (1981) who formulated the OFC as a variational problem and solved the optical flow field by minimizing the following cost function:

$$J=J_{\mathrm{o}}+\alpha\cdot J_{\mathrm{HS}} \tag{2}$$

where

$$J_{\mathrm{o}}=\iint\left[\frac{\partial I}{\partial t}+u\frac{\partial I}{\partial x}+v\frac{\partial I}{\partial y}\right]^2 dxdy \tag{3}$$

and J_{HS} is a global constraint on the smoothness of the gradient of the optical flow field:

$$J_{\mathrm{HS}}=\iint\left(|\nabla u|^2+|\nabla v|^2\right)dxdy \tag{4}$$

Here, α is a tunable parameter that determines the weight of the smoothness term.

In the VET algorithm (Germann & Zawadzki 2002), Lagrangian persistence is assumed for precipitation echoes during their movements, which is equivalent to the OFC equation (1). Different from the Horn and Schunck (1981) algorithm, VET calculates the total derivative of $I(x,y,t)$ by an upstream semi-Lagrangian scheme and uses a smoothness penalty function J_{WW} originally proposed by Wahba and Wendelberger (1980):

$$\begin{aligned}J_{\mathrm{WW}}=&\iint\left[\left(\frac{\partial^2 u}{\partial x^2}\right)^2+\left(\frac{\partial^2 u}{\partial y^2}\right)^2+2\left(\frac{\partial^2 u}{\partial x\partial y}\right)^2\right]dxdy\\&+\iint\left[\left(\frac{\partial^2 v}{\partial x^2}\right)^2+\left(\frac{\partial^2 v}{\partial y^2}\right)^2+2\left(\frac{\partial^2 v}{\partial x\partial y}\right)^2\right]dxdy\end{aligned} \tag{5}$$

To reduce the risk that the minimization converges towards secondary minima, a first guess is obtained through a scaling-guess procedure (Laroche & Zawadzki 1994), in which the motion field is iteratively retrieved with increasing grid resolution.

The MOVA algorithm is based on the original Horn and Schunck (1981) formalism with the smoothness constraint replaced by J_{WW} as in VET. The multi-grid treatment of VET (Germann & Zawadzki 2002) was also explored to handle the multi-scale motion of typical convective rainbands in southern China. Further implementation details are presented in Section 3 below.

Apart from the global approach used by the above variational algorithms, the aperture problem of OFC can also be resolved locally by, e.g. the local differential method introduced

by Lucas and Kanade (1981). In this method, the optical flow in a neighbourhood Ω of size ρ about a point p is assumed constant. The OFC evaluated at all the points q in the neighbourhood form the following system of linear equations:

$$I_x(q)\cdot u + I_y(q)\cdot v = -I_t(q) \qquad \text{where } q \in \Omega \qquad (6)$$

Here, $I_{x,y,t}(q)$ denotes the corresponding partial derivative evaluated at point q. Adopting a least-square principle and applying weights to different points in the neighbourhood through Gaussian convolution, Eq.(6) can be solved with the following solution:

$$\begin{pmatrix} u \\ v \end{pmatrix} = \begin{pmatrix} K_\rho * (I_x I_x) & K_\rho * (I_x I_y) \\ K_\rho * (I_y I_x) & K_\rho * (I_y I_y) \end{pmatrix}^{-1} \begin{pmatrix} -K_\rho * (I_x I_t) \\ -K_\rho * (I_y I_t) \end{pmatrix} \qquad (7)$$

where the operator $*$ denotes convolution and K_ρ a Gaussian kernel with standard deviation ρ. Compared with the global variational methods mentioned in previous paragraphs, the above local scheme is fast which mainly involves the calculation of partial derivatives for a 2x2 matrix. Due to the use of Gaussian convolution, the algorithm is robust against noise. As pointed out by Bowler *et al.* (2004), radar or rain rate field is typically noisy and pre-smoothing is needed for a stable calculation of the partial derivatives. One major drawback of this local method is that the resulting optical flow is mainly confined to the moving objects without any assessment on the motion vectors around them. For the prediction of the future position of the objects, say using the backward semi-Lagrangian advection scheme (Staniforth & Cote 1991), the motion assessment for the entire computational domain is needed.

For real-time image processing with a commodity desktop computer, Bruhn *et al.* (2003) introduced a new variational optical flow technique which combines the advantages of the global approach and local method. Besides a full multi-grid strategy is used to attain high accuracy and speed up the iterative solving of the system of linear equations. Different from the uni-directional coarse-to-fine cascading approach as adopted by the VET and MOVA algorithms, the full multi-grid strategy is bi-directional with errors at all coarser levels of the grid hierarchy corrected before going down to the next finer level. The smoothness constraint is the same as that of Horn and Schunck (1981). An in-depth description of this advanced optical flow technique is beyond the scope of this extended abstract and the interested readers are referred to the seminal papers by Bruhn *et al.* (2003; 2005).

3. IMPLEMENTATION IN SWIRLS

3.1 *Correlation Based Tracking*

In the first generation of SWIRLS, the motion vectors of rainfall systems were retrieved by tracking small blocks of reflectivity pixels in two successive radar images according to the TREC (Tracking of Radar Echoes by Correlation) method (Tuttle & Foote 1990). Technically, the movement of individual radar echoes between two consecutive CAPPI scans at 6 minutes apart was derived by maximizing the cross-correlation. The whole domain was divided into a number of equally sized blocks. For each block in the latest radar image, the cross-correlations with all possible blocks in the preceding 6 minutes were calculated to determine which block possessed the highest correlation. The vector joining these 2 blocks then represented the motion vector. To reduce computation time, a search radius, which tallies with the maximum possible speed of rainfall systems, was prescribed. The final output field would be filled and smoothed by Cressman analysis. In SWIRLS, the reflectivity field has a resolution of 480×480 pixels. The blocks are spaced 5 pixels apart, giving a TREC vector field on a 93 x 93 grid. The equivalent spatial resolution is of the order of 1 to 5 km depending on the range of the radar scan. Further technical details are described in Li *et al.* (2000) and Li & Lai (2004). Since the primary objective of SWIRLS is QPF, the input CAPPI fields to all tracking algorithms and subsequent extrapolation are chosen at 2-km altitude.

For prediction of thunderstorm movement over the Hong Kong Flight Information Region (HKFIR), an Aviation Thunderstorm Nowcasting System (ATNS) has also been developed by HKO (Li & Wong 2010). ATNS shares the same TREC algorithm of SWIRLS but it uses 3-km CAPPI for both tracking and extrapolation of radar echoes.

3.2 *Optical-flow Based Tracking*

Considering the limitation of TREC, MOVA was introduced in 2009 (Wong *et al*. 2009). In MOVA, the optical flow cascade has 7 levels with box size starting from full domain (256 km) down to around 3 km. There are a total of 7 weighting parameters to control the smoothness constraint term at each cascade level. They are tuned for optimal results in rainstorm situations. To maintain continuity between motion analyses, which is performed every 6 minutes following the radar scan update cycle, three consecutive radar reflectivity pictures at 6-min intervals are used to construct and calculate the OFC cost function, i.e.:

$$J_o = J_o(T_{-12\,\mathrm{min}} \text{ to } T_{-6\,\mathrm{min}}) + J_o(T_{-6\,\mathrm{min}} \text{ to } T_0)$$

More technical details can be found in Wong *et al.* (2009) and Wong (2012).

It has been noticed that MOVA tends to underestimate flow speed while the direction is mostly accurately determined. One possible reason could be attributed to the fact that spatial smoothing is not applied to the radar images nor their partial derivatives. For rapidly evolving convective rainfall, which is commonplace in and around Hong Kong during the monsoon seasons, the jumpiness of the radar echoes could render the calculation of partial derivatives inaccurate and thus exerts negative impact to the solution of the OFC. Bowler *et al.* (2004) also pointed out that it is necessary to smooth the radar rain-rate fields in order to obtain a stable estimate of the derivatives.

Based on the combined local-global full multi-grid variational optical flow technique put forward by Bruhn *et al.* (2003) for real-time applications, a new scheme for tracking radar echoes is currently under development in the Observatory with a view to addressing the weakness experienced by MOVA. For easy discussion, the new scheme is conveniently referred to as ROVER (Real-time Optical flow by Variational methods for Echoes of Radar). Besides more robustness against noise as inherited from the local method, the number of tunable parameters as embedded in the new technique is reduced to a more manageable set of three, namely σ, ρ and α, which are used throughout the multi-grid hierarchy. Here, σ and ρ represent respectively the standard deviations in the Gaussian kernels for image pre-smoothing and the weights in the structure tensor of the local method. The third parameter α is the same weight parameter commonly used in the global optical flow methods to control the relative importance of the smoothness constraint. For the ROVER scheme currently under testing, these parameters were tuned for optimal QPF results using squall line cases. Squall lines are typically fast moving and long lasting with high intensity along and sharp gradient across their rainbands when rendered as images. With these properties, they are considered ideal for testing and tuning tracking algorithms.

Following Germann and Zawadzky (2002), fields of radar reflectivity factor Z, instead of rain rate, are chosen to be converted to images for optical flow analysis in ROVER. Considering the significant smoothing effects incurable by image pre-smoothing and Gaussian convolution, the reflectivity factor in 0-60 dBZ is converted non-linearly to a gray scale of 0-255 using the following function:

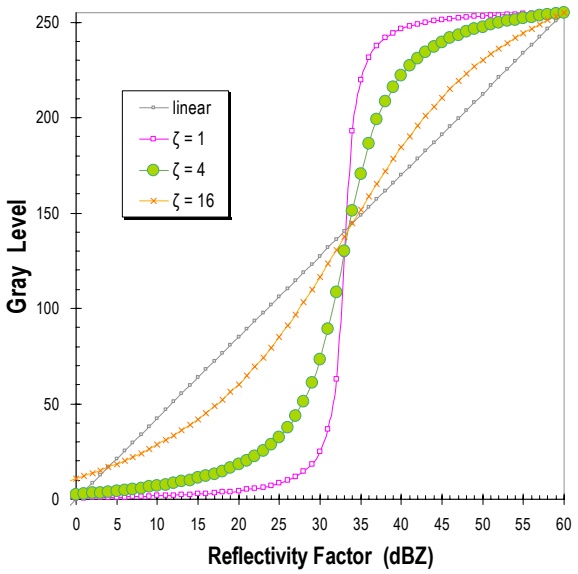

Fig. 1 *Different transformations for mapping reflectivity factor (0-60 dBZ) to gray levels (0-255).*

$$G(Z) = \tan^{-1}\left(\frac{Z - Z_c}{\zeta}\right)$$

Here, the parameter Z_c specifies the point of inflection and is chosen in ROVER to be 33 dBZ, which is currently adopted as the threshold for identification of significant convection in aviation forecasting in Hong Kong. The other parameter ζ controls the sharpness of the inflection and the gray levels on both sides of the inflection point. Fig. 1 shows three example curves with ζ set to 1, 4 and 16 dBZ. In general, smaller ζ implies sharper inflection (e.g. the purple curve with $\zeta = 1$ dBZ) and vice versa. As illustrated by the orange curve with $\zeta = 16$ dBZ, the transformation becomes more like a linear one (the gray diagonal line refers) as ζ increases. With the general shape illustrated in Fig. 1, this kind of non-linear transformation can highlight echoes from the convective regime with high dBZ values and play down echoes with intensity of less interest. With such preferential enhancement (suppression) of brightness for the most intense (less critical) parts of convective rainbands, the structure and gradient of precipitation radar images can be better preserved when subjected to subsequent smoothing treatments in ROVER. From case studies, the sharpness parameter was chosen to be 4 dBZ.

(a)

(b)

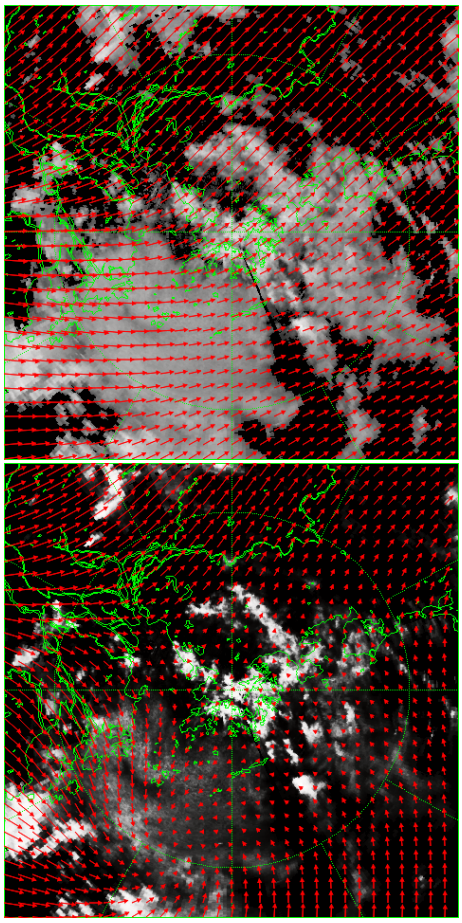

Fig. 2 *Tracking example by ROVER illustrating the effect of different Z-G transformations: (a) linear; (b) non-linear. Reflectivity rendered in gray scales. Red arrows represent the resulting optical flow vectors. Coastlines are drawn in green. Hong Kong is located in the middle part of the map. Based on 2-km CAPPI at 1012 and 1018 LST on 22 May 2011.*

Fig. 2 shows an example on 22 May 2011, illustrating the difference in transformed brightness and tracked motion vectors resulting from the use of linear and non-linear Z-G transformations. In this example, intense convection was developing from a quasi-stationary surface trough of low pressure lingering along the coastal areas of southern China. The developed convection was steered by the upper southwesterly winds. For the linearly transformed reflectivity shown in Fig. 2(a), individual convective cells were not distinctive and the resulting optical flow depicted generally the steering flow acting on the rainband as a whole. When the convection was made prominent through non-linear transformation, ROVER was able to focus more on the motion of individual cells. The resulting optical flow near and over

(a)

(b)

(c)

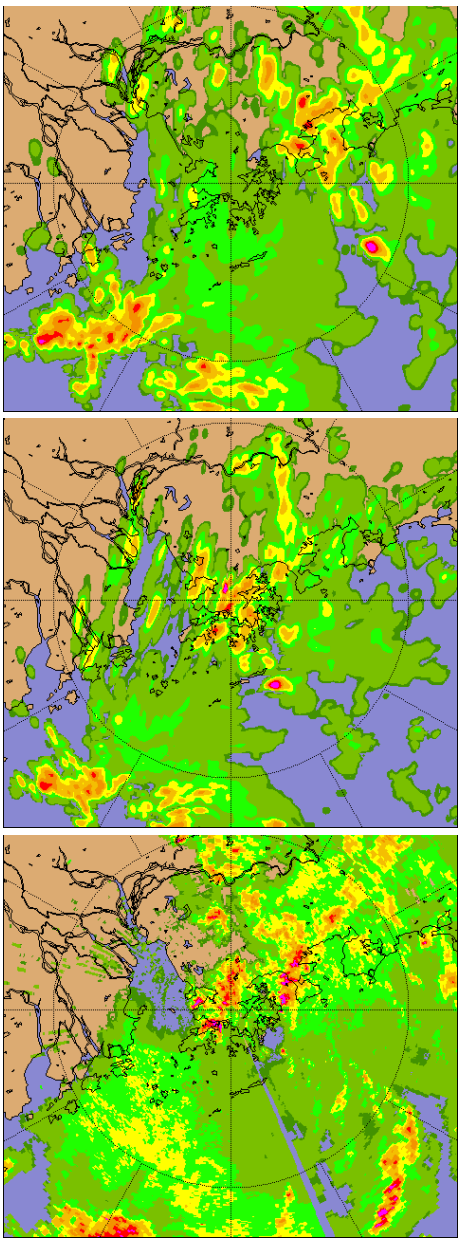

Fig. 3 *Three-hour extrapolated reflectivity fields for the case shown in Fig.2: (a) linear; (b) non-linear with inflection point at 33 dBZ; (c) .actual radar reflectivity three hours later. For easy visualization of convective cells, yellow to red colours indicate 34 dBZ or above.*

Hong Kong became much weakened and confluent, better reflecting the quasi-stationary nature of the underlying surface trough.

Shown in Fig.3(a) and 3(b) are the corresponding 3-hour extrapolated reflectivity fields, which indicated a large difference in the strength of convection over Hong Kong.Comparing with the actual reflectivity at the valid time as shown in Fig.3(c), the convective development areas indeed was quasi-stationary

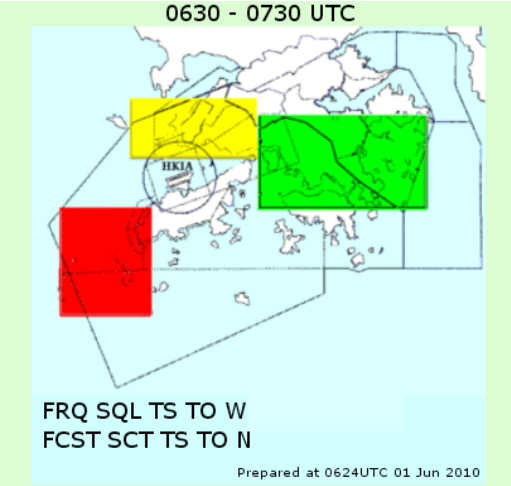

Fig. 4 Sample graphical and text display of significant convection forecast over the arrival and departure corridors of HKIA for the next hour. The circle marks the aerodrome area (8 km from the Aerodrome Reference Point) of HKIA.

during that period. Although there also involved echo dissipation and re-development during the 3-hour period, the forecast as shown in Fig.3(b) is regarded as generally more realistic than that in Fig.3(a).

4. APPLICATION TO CONVECTION NOWCAST FOR AVIATION

In SWIRLS, QPF is obtained basically by the extrapolation and accumulation of the observed reflectivity field converted suitably into rainfall rate (Li 2009, Li *et al.* 2000). The extrapolation is performed by using a backward semi-Lagrangian advection scheme (Staniforth & Cote 1991). For convection nowcast, the same extrapolation scheme is used and the products of interest are simply the extrapolated reflectivity fields themselves. As mentioned in section 3, there are currently four different radar echo-tracking systems, namely TREC, MOVA, ROVER and ATNS, and hence four possible sets of reflectivity forecasts available for the development of significant convection nowcast guidance for the arrival and departure corridors of the Hong Kong International Airport (HKIA).

In support of the air traffic management by Air Traffic Control (ATC) in severe weather situations, 1-hour forecasts of significant convection over key ATC areas for arrival, departure and missed approach flights (colour marked areas to the east, west and north of HKIA in Fig. 4) are provided to ATC every 6 minutes through an integrated webpage for "Significant Convection Monitoring and Forecast".

Table 1: Conversion algorithm from pictorial to textual warning messages.

Currently Observed status	Forecast status	Textual message
GREEN	RED	FCST FRQ TS
YELLOW	RED	SCT TS **INTSF**
RED	RED	FRQ TS
GREEN	YELLOW	FCST SCT TS
YELLOW	YELLOW	SCT TS
RED	YELLOW	FRQ TS **WKN**
GREEN	GREEN	
YELLOW	GREEN	SCT TS **WKN**
RED	GREEN	FRQ TS **WKN**

4.1 *Automated Products*

The significant convection forecast product is presented in both pictorial and textual forms as shown in Fig. 4. The thresholds for defining the pictorial "yellow" and "red" alerts were being tuned to the effect that "yellow" means medium impact where aircraft could still fly by the intense convection or fly in between the gaps, and "red" means high impact where the convection almost completely blocks the way of aircraft. If no significant convection is forecast or if there is just an isolated thunderstorm with a small extent over the region, the color code will be "green".

Specifically, the colour status of each of the three strategic areas is determined using the following set of criteria based on radar reflectivity data at 3-km height:

"*yellow*": at least 50% of the area concerned is covered by echoes with intensity ≥ 33 dBZ or at least 4% covered by echoes with intensity ≥ 41 dBZ.

"*red*": at least 10% of the area concerned is covered by echoes with intensity ≥ 41dBZ.

The final forecast color status of the area will be the most significant color status among the 10 forecasts extrapolated in steps of 6 minutes within the next one hour.

Textual forecasts are added to the bottom of the pictorial display if significant convection is forecast over the arrival and departure corridors. The wordings are presented in a standardized protocol as agreed with ATC. For examples, the code "TS" is used to represent significant convection including

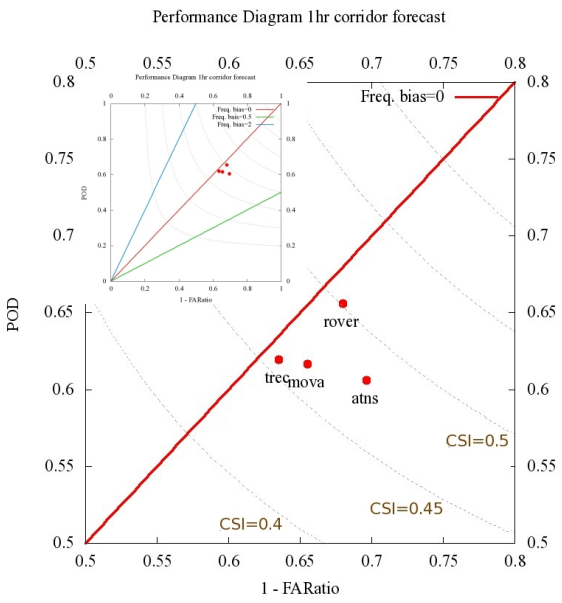

Fig. 5 Performance Diagram showing the verification results of significant convection forecast for the arrival/departure corridors in Hong Kong. The x-axis refers to one minus the false alarm ratio (1-FARatio) The y-axis is the probability of detection (POD), with a perfect forecast indicated by a point on the upper-right corner (1,1). Dashed curves on the Performance Diagram mark the CSI isopleths. The inset is the full-scale diagram with blue and green line indicating respectively a frequency bias of 2 and 0.5. The main plot is a "zoom-in" of the inset.

thunderstorm. When translated to textual products, the pictorial "green" means either "no convection" or "isolated convection" forecast with a blank message, while "yellow" and "red" respectively indicates "SCT" (scattered) and "FRQ" (frequent) convection forecast over the specified region. Squall line (coded "SQL"), when manually issued by the Aviation Forecaster, takes higher priority than "FRQ" and will also be shown in red color in pictorial presentation. Forecast of intensity change is generated based on the difference between observation and forecast status. If the observed status is "yellow" and the forecast is "red", then the code "INTSF" (intensify) will be generated, whereas if the observed status is higher than that of the forecast, "WKN" (weaken) will be used. The automatic conversion algorithm is summarized in Table 1.

4.2 *Verification of Automated Products*

To assess the performance of the automated products, systematic verification has been conducted for the period of June-October 2011. Since the forecast is presented as colour status for the next hour, the ground truth for verification is taken as the highest analyzed colour status from the corresponding actual radar images. The same set of criteria used for producing warnings applies here. Note that only 3-km CAPPI are used in the verification, despite the fact that the motion-vector fields from TREC and MOVA are generated from 2-km CAPPI. The possible impact of this mismatch will be discussed in the next section.

Probability of Detection (POD), False Alarm Ratio (FAR) and Critical Success Index (CSI) for dichotomy forecasts are adopted as performance measures. "Green" and non-"green" forms the dichotomy in the contingency tables for each of the nowcasting algorithms. In other words, a hit means either Yellow or Red status is forecast and verified correct by subsequent radar observations. Conversely, a false alarm means the actual status remains "green". The verification results over the whole study period can be compactly visualized using Performance Diagram (Roebber 2009) as shown in Fig. 5. It was found that within a lead time of one hour, the CSI for various nowcasting algorithms ranges from 0.4 to 0.5 with ROVER performed the best (closer to the top-right corner of the Performance Diagram). ATNS performed next to ROVER in terms of CSI but exhibited a characteristic frequency bias significantly lower than the others (leaning closer to the green straight line on the Performance Diagram). Therefore, its CSI was achieved through lowering false alarm ratio at the expense of POD.

5. DISCUSSIONS

As ATNS used 3-km CAPPI whereas other nowcasting methods used 2-km CAPPI, there would always be some differences in the resulting forecast reflectivity field even if all else were equal. The fact that the verification ground truth was taken also from 3-km CAPPI would unavoidably favour ATNS nowcast to a certain extent. As pointed out in the previous section, the relatively high CSI of ATNS was achieved with a low frequency bias relative to the others. This might be attributed to the use of 3-km CAPPI in ATNS. Whilst this study could not isolate the relative merits of tracking and intensity, more detailed study, e.g. with the use of 3-km CAPPI in all algorithms of SWIRLS, could be conducted in the future to confirm the relative skillfulness of ATNS over TREC and MOVA. It is also of practical interest to see if ROVER could achieve even higher scores when the "correct" reflectivity is used.

As shown in Table 1, the textual forecasts are more refined when compared with their pictorial counterparts. As such, the samples collectable for each textual possibility are relatively scarce and their verifications were therefore not

Fig. 6 Screen capture of the combined nowcast viewer in time-staggered display mode with forecasts aligned according to valid times. Each row corresponds to the actual radar observation and the 10 nowcasts from a single run of the selected nowcasting algorithm. The rows are time-ordered with the latest one on top.

pursued.

Convection initiation, growth and decay are not catered for in all nowcast products at present. The Aviation Forecaster would make use of actual observations and apply conceptual models to forecast the development of significant convection over the area of concern. Forecasters noted that the present echo-tracking methods may tend to under-forecast the speed of movement of squall line from the northwest or north in which the group velocity and phase velocity of individual echoes are in different directions. This is especially so for forecasts based on TREC method in SWIRLS/ATNS. When an organized line of convection or squall line is approaching Hong Kong, apart from cautious use of the tracked speed, the Aviation Forecaster would also cater for possible accelerating motion and/or echo development ahead of the front edge of the intense line echoes when they approach HKIA.

To facilitate timely human intervention to the automated products, a web interface was developed for forecasters to modify interactively the significant convection forecast for the arrival/departure corridors. This approach of taking human forecasters into the loop of a real-time automatic system is termed "human-machine-mix" mode of operation. ATNS forecast is taken as the default of the computer-generated forecast but the Aviation Forecaster can select alternative forecasts generated from TREC, MOVA, or ROVER of SWIRLS, considering their strengths and weaknesses for tracking different types of convective systems. To facilitate inter-comparison, products of all nowcasting algorithms are displayed as stamp maps in a combined nowcast viewer (Fig. 6). Forecasts presented in this compact manner also enable comprehension by forecasters from an ensemble approach.

Through discussions with forecasters and some simulated cases for drill, the "human-machine-mix" product was believed to have both higher POD and FAR. This is because forecasters, who can focus more on convection initiation using other meteorological hints, will be more readily able to detect the occurrence (and growth as well) of significant convection. But for the same reason, they may introduce more false alarms due to the uncertainties in the exact locations and intensities of the significant convection. Verification of this product would be conducted to see whether forecasters have added value to the computer generated product.

6. CONCLUDING REMARKS

With the use of an advanced optical flow algorithm and a special pre-processing procedure geared for convective rainbands, the nowcast products from ROVER of SWIRLS were apparently more skillful than other algorithms available at the Observatory. When further supportive statistics are collected in coming rain seasons, ROVER nowcast products will be considered for adoption as the operational default in significant convection nowcast for the terminal areas in Hong Kong subject to verification results. Verification of QPF based on the various tracking algorithms are underway and ROVER will be assessed for its relative merits over MOVA or TREC. Looking further ahead, research studies will be pursued to enhance the tracking by ROVER in even more difficult situations such as translating-rotating storms typical of tropical cyclones.

ACKNOWLEDGEMENT

The authors would like to thank Ms Queenie Lam and Mr. S.T. Chan for their valuable comments and suggestions on this manuscript. Thanks also went to Mr. Vincent Cheng and Mr. Marcos Mak for their technical assistance in this research.

REFERENCE

Aubert, G., R. Deriche, and P. Kornprobst, 1999: Computing optical flow via variational techniques. *SIAM J. Appl. Math.*, **60**, 156-182.

Beauchemin, S.S. and J.L. Barron 1995: The computation of optical flow. *ACM Computing Surveys*, vol. **27**, issue 3, p 433-467.

Bowler, N.E., C.E. Pierce and A. Seed, 2004: Development of a precipitation nowcasting algorithm based upon optical flow techniques. *J. Hydrol.*, **288**, 74–91.

Bowler, N.E., C.E. Pierce and A. Seed, 2006: STEPS: A probabilistic precipitation forecasting scheme which merges an extrapolation nowcast with downscaled NWP. *Q. J. R. Meteorol. Soc.*, **132**, 2127–2155.

Bruhn, A., J. Weickert, C. Feddern, T. Kohlberger and C. Schnörr, 2003: Real-time optic flow computation with variational methods. In N. Petkov, M. A. Westenberg (Eds.): Computer Analysis of Images and Patterns. *Lecture Notes in Computer Science*, Vol. **2756**, Springer, Berlin, 222-229.

Bruhn, A., J. Weickert, C. Feddern, T. Kohlberger, C. Schnörr, 2005: Variational optic flow computation in real-time. *IEEE Transactions on Image Processing*, Vol. **14**, No. 5, 608-615.

Civil Aviation Department, HKSARG, 2012: Aeronautical Information Publication (AIP). Available online at: http://www.hkatc.gov.hk .

Fleet, D.J. and A.D. Jepson, 1990: Computation of component image velocity from local phase information. *International Journal of Computer Vision*, **5**, 77-104.

Germann, U. and I. Zawadzki, 2002: Scale-Dependence of the Predictability of Precipitation from Continental Radar Images. Part I: Description of the Methodology. *Mon.Wea.Rev.*, **130**, 2859–2873.

Horn, B. and B. Schunck, 1981: Determining optical flow. *Artificial Intelligence*, **17**, 185–203.

Laroche, S., and I. Zawadzki, 1994: A variational analysis method for retrieval of three-dimensional wind field from single-Doppler radar data. *J. Atmos. Sci.*, **51**, 2664–2682.

Laroche, S., and I. Zawadzki, 1995: Retrievals of horizontal winds from single-Doppler clear-air data by methods of cross correlation and Variational analysis. *J. Atmos. Oceanic Technol.*, **12**, 721–738.

Li, P.W., W.K. Wong, K.Y. Chan & Edwin S.T. Lai, 2000: SWIRLS — An Evolving Nowcasting System. *Hong Kong Observatory Technical Note*, No.100.

Li, P.W., & E.S.T. Lai, 2004: Short-range Quantitative Precipitation Forecasting in Hong Kong. *J. Hydrol.*, **288**, 189-209.

Li, P.W. & D.S. Lau, 2008: Development of a Lightning Nowcasting System for Hong Kong International Airport. *13th Conference on Aviation, Range and Aerospace Meteorology, New Orleans, Louisiana, USA, 20-24 January 2008*

Li, P.W., 2009: Development of a Thunderstorm Nowcasting System in Support of Air Traffic Management. *AMS Aviation, Range, Aerospace Meteorology Special Symposium on Weather-Air Traffic Management Integration, Phoenix, Arizona, USA, 11-15 January 2009*

Li, P.W. & W.K. Wong, 2010: Development of an Advanced Aviation Nowcasting System by Including Rapidly Updated NWP Model in Support of Air Traffic Management. *The 14th Conference on Aviation, Range, and Aerospace Meteorology, AMS, Atlanta, Georgia, USA, 17-21 Jan 2010*

Lucas, B.D. and T. Kanade, 1981: An iterative image registration technique with an application to stereo vision. *Proceedings of Seventh International Joint Conference on Artificial Intelligence*, p 674-679, Vancouver, Canada, August 1981.

Roebber, P.J., 2009: Visualizing Multiple Measures of Forecast Quality. *Wea. Forecasting*, **24**, 601-608.

Srivastava, K., S.Y. Lau, H.Y. Yeung, T.L. Cheng, R. Hardwaj, A.M. Kannan, S.K.R. Bhowmik and H. Singh, 2012: Use of SWIRLS nowcasting system for quantitative precipitation forecast using Indian DWR data. *MAUSAM Quarterly Journal of Meteorology, Hydrology & Geophysics*, Vol.**63**, No.1, Page 1-16.

Staniforth, A., J. Cote, 1991: Semi-Lagrangian Integration Schemes for Atmospheric Models — A Review. *Mon. Wea. Rev.*, **119**, 2206–2223.

Tuttle, J.D., Foote, G.B., 1990: Determination of the boundary layer airflow from a single Doppler radar. *J. Atmos. Ocean. Technol.* **7**, 218–232.

Wahba, G. and J. Wendelberger, 1980: Some new mathematical methods for variational objective analysis using splines and cross validation. *Mon. Wea. Rev.*, **108**, 1122–1143.

Wong, Wai-kin, Linus H.Y. Yeung, Ying-chun Wang & Min Chen, 2009: Towards the Blending of NWP with Nowcast — Operation Experience in B08FDP. *WMO Symposium on Nowcasting*, 30 Aug-4 Sep 2009, Whistler, B.C., Canada.

Wong, W.K. 2012: Challenges and Developments in Very-short range Forecast of Significant Convection for Aviation Applications in Hong Kong.

(submitted) *The 46th Congress of the Canadian Meteorological and Oceanographic Society / 21st AMS Conference on Numerical Weather prediction and the 25th AMS Conference on Weather Analysis and Forecasting*, 29 May-1 June, Montreal, Canada.

World Meteorological Organization (WMO), 2012: *WMO Report on Final Review Meeting for the World EXPO 2010 Nowcasting Services (WENS) Demonstration Project and Capacity-Building Workshop*, 14-18 November 2011, Shanghai, China.

Yeung, Linus H.Y., W.K. Wong, Philip K.Y. Chan & Edwin S.T. Lai, 2009: Applications of the Hong Kong Observatory nowcasting system SWIRLS-2 in support of the 2008 Beijing Olympic Games. *WMO Symposium on Nowcasting*, 30 Aug-4 Sep 2009, Whistler, B.C., Canada.